

Spray-Layer-by-Layer Carbon Nanotube/Electrospun Fiber Electrodes for Flexible Chemiresistive Sensor Applications

Kittipong Saetia, Jan M. Schnorr, Matthew M. Mannarino, Sung Yeol Kim, Gregory C. Rutledge, Timothy M. Swager, and Paula T. Hammond*

Dedicated to the memory of Officer Sean Collier for his caring service to the MIT community and for his sacrifice

Development of a versatile method for incorporating conductive materials into textiles could enable advances in wearable electronics and smart textiles. One area of critical importance is the detection of chemicals in the environment for security and industrial process monitoring. Here, the fabrication of a flexible, sensor material based on functionalized multi-walled carbon nanotube (MWNT) films on a porous electrospun fiber mat for real-time detection of a nerve agent simulant is reported. The material is constructed by layer-by-layer (LbL) assembly of MWNTs with opposite charges, creating multilayer films of MWNTs without binder. The vacuum-assisted spray-LbL process enables conformal coatings of nanostructured MWNT films on individual electrospun fibers throughout the bulk of the mat with controlled loading and electrical conductivity. A thiourea-based receptor is covalently attached to the primary amine groups on the MWNT films to enhance the sensing response to dimethyl methylphosphonate (DMMP), a simulant for sarin nerve agent. Chemiresistive sensors based on the engineered textiles display reversible responses and detection limits for DMMP as low as 10 ppb in the aqueous phase and 5 ppm in the vapor phase. This fabrication technique provides a versatile and easily scalable strategy for incorporating conformal MWNT films into three-dimensional substrates for numerous applications.

functionalities, including flexibility, lightweight, and stretchability, enable new device designs for many applications previously unfeasible with conventional electronics technology. Examples of these novel applications include wearable displays,^[2a] health monitoring,^[2b] energy storage devices,^[2c] security, and environmental monitoring.^[2d] One area of critical importance is chemical sensing due to the increased threat of chemical terrorism at the domestic and international level. Chemical warfare agents (CWAs), especially nerve agents such as tabun (GA), sarin (GB), soman (GD), and VX, are of great concern due to their acute toxicity at low concentration and colorless characteristics. Soldiers and emergency responders are particularly susceptible such harmful environments. Laboratory-based analytical techniques, such as chromatography and spectroscopy, are not suited for in-field use because they require bulky equipment and considerable skills to operate. Wearable sensors that continuously detect toxic chemicals in the surrounding environment

in real time can offer advantages over laboratory-based analytical methods and hand-held devices because the wearers can receive timely information without having to operate a complex device or compromising the functionality and discomfort of their garments. To achieve high-performance wearable sensor with good sensitivity and selectivity, the sensing device needs to have the following characteristics: simple architecture to remain lightweight and portable, high surface area for enhanced interaction, and chemical functionality to achieve selective response.

Carbon nanotube (CNT) resistance-based chemical sensors have been extensively investigated in recent years, and they are recognized as highly sensitive chemical sensors.^[3] A typical CNT-based chemiresistor consists of one or several pairs of electrodes that make electrical contact with a thin film or network of CNTs. A change in the electrical resistance of the CNT film upon exposure to an analyte is measured as the output signal. The advantages of chemiresistors include minimal electronic

1. Introduction

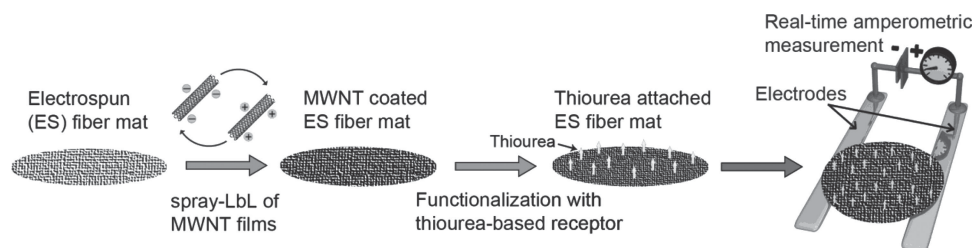
Wearable electronics can be defined as portable electronic devices that can be seamlessly incorporated into the user's outfit as part of the clothing or accessory.^[1] Their unique

K. Saetia, Dr. M. M. Mannarino, Dr. S. Y. Kim, Prof. G. C. Rutledge, Prof. P. T. Hammond
Department of Chemical Engineering and Institute for Soldier Nanotechnologies
Massachusetts Institute of Technology
Room 76-553, 77 Massachusetts Ave
Cambridge, MA 02139, USA
E-mail: hammond@mit.edu

Dr. J. M. Schnorr, Prof. T. M. Swager
Department of Chemistry and Institute for Soldier Nanotechnologies
Massachusetts Institute of Technology
Cambridge, MA 02139, USA



DOI: 10.1002/adfm.201302344



Scheme 1. Schematic representation of the fabrication steps of a chemiresistive sensor based on MWNT-film coated electrospun fiber mat.

components, low power consumption, and simple operation.^[3d] These features enable miniaturization of the sensing unit and unobtrusive integration into a lightweight, wearable system. There are three general methods for fabricating CNT-based resistive sensors: 1) directly growing CNTs using vapor deposition, 2) transferring a CNT array or CNT thin film, and 3) solution-depositing CNT suspension, such as drop-cast, spin-coat, and ink-jet, on a rigid (glass or silicon wafer) or flexible plastic substrate.^[4] Although these fabrication techniques can generate CNT network with various geometries and structures, they do not allow uniform, scalable deposition of CNT film on a porous, textile material, which is an ideal substrate for wearable electronics due to its flexible and breathable characteristics. Fabrics made of electrospun (ES) polymeric fibers provide flexible, porous scaffolds with high surface area, which enhances the specific surface area of the sensing material. The utilization of ES fiber mats as sensor substrates has been shown by Wang et al.^[5a] and Bhattacharyya et al.^[5b] for fabrication of polymer-based biosensors to improve sensitivity and response time due to enhanced surface area. These studies suggest that an electrospun fiber mat is an ideal candidate as a non-conducting substrate for fabrication of a chemiresistive sensor and also serves as a platform for a wearable electronics system.

The layer-by-layer (LbL) assembly technique is a versatile method for creating uniform thin films through sequential adsorption of complementary multivalent species on a substrate via electrostatic interactions, hydrogen bonding, or other secondary interactions.^[6] A substrate with an innate charged surface is successively dipped into solutions of oppositely charged species, which adsorb to the developing film. This approach enables a fine control over the composition and structure of the LbL films by adjusting the assembly conditions (e.g., salt concentration, pH), as well as a diverse choices of components that can be incorporated into the thin films.^[7] In our previous work, we have extended this LbL technique by spraying solutions of charged species, such as polyelectrolytes and nanoparticles, onto a porous ES fiber mat in conjunction with a pressure gradient across the substrate to deposit uniform coatings composed of polyelectrolytes and nanoparticles on individual fibers throughout the bulk of the ES fiber substrate.^[8] Spray-LbL coating of porous non-wovens provides a rapid, scalable approach to introduce new functionalities to materials while retaining their mechanical robustness. In addition, we have demonstrated the ability to construct multi-walled carbon nanotube (MWNT) multilayer films without binder on planar substrates and carbon paper using conventional dip-LbL^[9] and spray-LbL,^[10] respectively, to create electrodes for energy storage

applications. These studies suggest that the LbL technique is well suited for depositing conformal MWNT films on porous ES fiber substrates.

Recently, dip-LbL assembly has been utilized to deposit CNTs and graphene on electrospun fiber mats.^[11] However, the LbL films in these studies contain polymer as part of the multilayers, which functions as a binder to facilitate the LbL assembly process. Spray-LbL assembly of binder-free CNT films provides a more versatile and rapid approach to obtain nanostructured thin films composed of only CNTs. The resulting systems provide access to the surfaces of the functionalized carbon nanotubes, which is key to achieving high levels of active surface area as binding sites for sensing. An added advantage of spray-LbL is the ability to control the coating of fine pore within the electrospun mat without introducing bridging across pores, thus limiting accessible surface area with increased film thickness. In this work, we present the design and fabrication of flexible, real-time chemiresistive sensors based on conformal LbL all-MWNT films on ES fiber mats. The sensory material is composed of two high-surface-area materials: functionalized MWNTs as a sensing component and an ES fiber mat as a flexible, porous substrate. **Scheme 1** depicts a schematic representation of the steps involved in the fabrication of this chemiresistive sensor. Here, we demonstrate the facility of the vacuum-assisted, spray-LbL technique to generate conformal, binder-free MWNT films on ES fibers to yield a MWNT/ES fiber electrode with electrical conductivity that can be varied with MWNT loading. The available functional groups on the MWNT films are used to covalently attach a thiourea-based receptor to the MWNT/ES fiber electrode to enhance sensitivity, and the thiourea-functionalized composite electrode is employed as a chemiresistive sensor for detecting dimethyl methylphosphonate (DMMP), a sarin nerve agent simulant, in both aqueous and gas phases. We believe this fabrication approach is a versatile, scalable method to generate flexible, high-surface-area CNT devices for applications ranging all the way from wearable sensors to energy storage devices.

2. Results and Discussion

2.1. Fabrication and Characterization of MWNT-Film-Coated Electrospun Fiber Mats

Figure 1 illustrates the steps involved in the fabrication of MWNT film-coated electrospun (ES) fiber mats. Parallel-plate

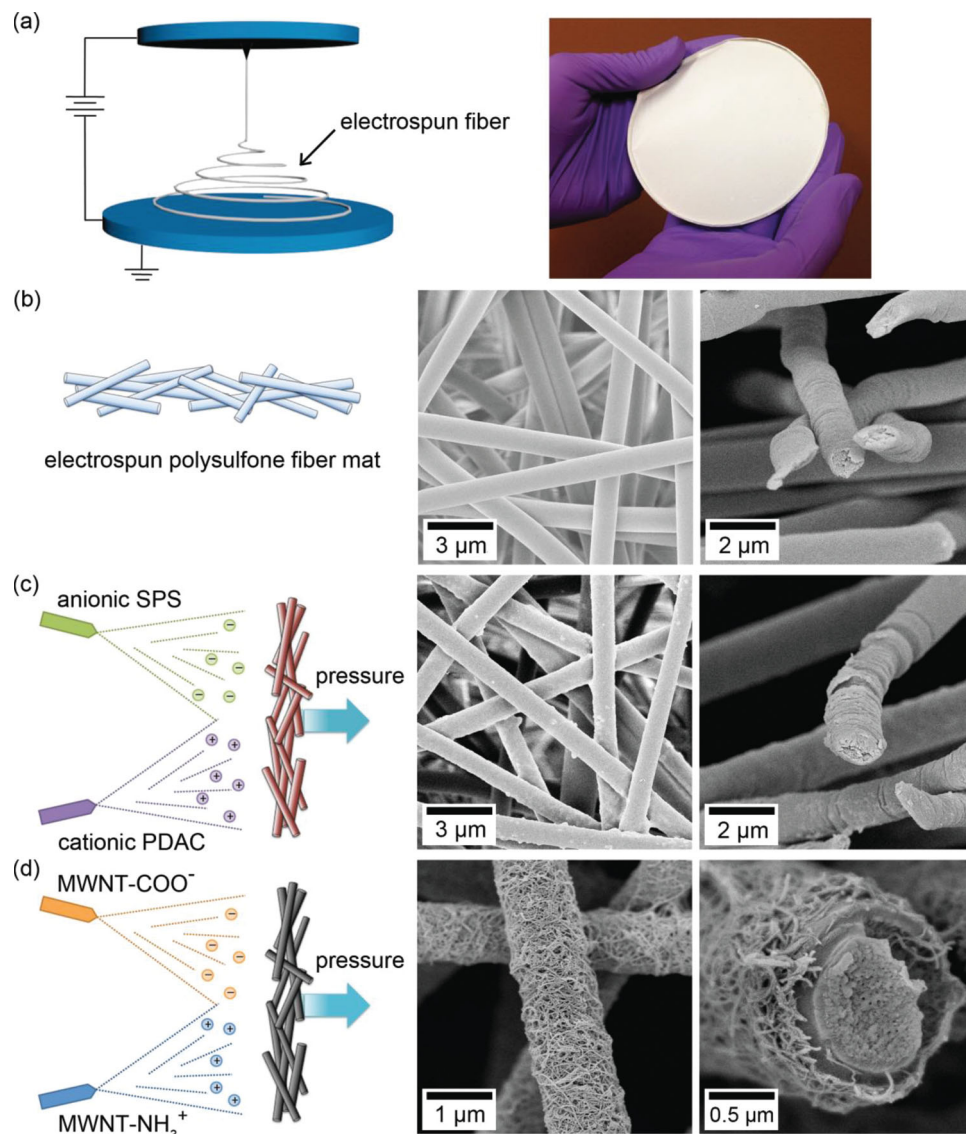


Figure 1. Illustration of layer-by-layer assembly on electrospun (ES) fiber mat. a) Parallel-plate electrospinning technique (diagram, left) is employed to create polysulfone ES fiber mats of 5–6 inch diameter (digital image, right). b) Schematic representation (left) and top-down (center) and cross-sectional (right) scanning electron microscopy (SEM) images of the annealed polysulfone ES fiber mat. c) A spray-LbL deposition technique with a pressure imposed across the mat is demonstrated to create conformal coatings of (SPS/PDAC)₁₀ thin films on individual fibers. d) (MWNT-COO⁻/MWNT-NH₃⁺)₁₅ films are uniformly coated on ES fibers independent of spray direction, as shown in the cross-sectional SEM image.

electrospinning apparatus (Figure 1a) was used to create flexible nonwoven mats of polysulfone fibers (average fiber diameter of $1.69 \pm 0.17 \mu\text{m}$ and mat thickness = $103 \pm 2 \mu\text{m}$, Figure 1b) from organic polymer solutions using a protocol modified from a previous report.^[12] Polysulfone was chosen as a polymer substrate because it has high chemical resistance and good thermal and mechanical stability.^[13] The nonwoven mats have an inherently high porosity of $85.1 \pm 1.1\%$, which was determined by a gravimetric method described elsewhere.^[12] Once the ES fiber mat was generated, it was first treated with one minute of air plasma to improve the wettability by introducing hydroxyl and charged carboxylated groups on the surface.^[14] The ES fiber mat was then immediately immersed into a

0.2 wt% aqueous solution of branched polyethylenimine (BPEI) for 10 min to impart positive charge on the surface of ES fibers. Ten bilayers of poly(sodium 4-styrene-sulfonate) (SPS) and poly(diallyldimethylammonium chloride) (PDAC) film were deposited on the ES fiber mat as base layers to facilitate a more effective electrostatic assembly of MWNT films by creating uniformly charged surfaces on the ES fibers. To achieve conformal coating on the ES fiber mat, we employed the vacuum-assisted spray-LbL technique described in previous work,^[8a] which forces flow throughout the porous membrane. By selecting the flow rate that yields Re_d (Equation 1, below the critical value of 6, where Re_d is the Reynolds number based on a cylinder diameter for flow separation from the downstream side of the

cylinder,^[15] uniform films can be created on the ES fibers. At $Re_d > 6$, LbL film growth has been observed only near the stagnation point on the front of the ES fibers.^[8a] The flow rate was adjusted in this work to give an $Re_d = 1.4$, which allowed conformal films to be developed on the ES fibers. Ten base layers of (SPS/PDAC) were deposited by alternately spraying aqueous solutions of 10 mM SPS and PDAC (pH 4) onto the ES substrate to coat the ES fibers uniformly with (SPS/PDAC)₁₀ films with a total thickness of ≈ 25 nm (Figure 1c).

$$Re_d = (DV_s)/[(1 - \varepsilon) v] \quad (1)$$

where D is the diameter of ES fibers, V_s is the superficial fluid velocity, $\varepsilon = 0.85$ is the void fraction of the ES fiber mat, and $v = 15.7 \times 10^{-6} \text{ m}^2 \text{ s}^{-1}$ is the kinematic viscosity of air at 300 K.^[8a]

To create electrostatic LbL films of MWNTs, negatively and positively charged MWNT suspensions were prepared by chemical functionalization of the MWNT surfaces based on previous reports (See reaction scheme in Supporting Information).^[9,13] In brief, carboxylic acid groups were created at defect sites and ends of unmodified MWNTs through acid oxidation to impart aqueous solubility and anionic surface character (MWNT-COO⁻). Positively charged MWNTs with free amine groups were prepared by introducing amine groups through a carbodiimide-mediated coupling reaction of MWNT-COO⁻ and ethylenediamine to form MWNT-NH₃⁺. X-ray photoelectron spectroscopy (XPS) elemental analysis was performed to verify the surface functional groups on the modified MWNTs (Figure S2a,b, Supporting Information). The XPS analysis of the C_{1s} spectra for the unmodified MWNTs, MWNT-COO⁻, and MWNT-NH₃⁺ shows detailed surface functional groups on the MWNTs (Figure S2c, Supporting Information). The unmodified MWNTs consisted of primarily sp²-hybridized carbons centered at 284.5 eV (in red) and some sp³-hybridized carbons centered at 285.2 eV (in magenta). Additional peaks at higher energies indicated small traces of C–O (286.2 \pm 0.1 eV) and carbonyls C=O (286.8 \pm 0.2 eV).^[9] These oxygen-containing groups on the unmodified MWNTs were attributed to atmospheric oxidation and residual oxides resulting from the MWNT synthesis process.^[16] The C_{1s} peak of MWNT-COO⁻ shows two additional higher binding energies that were attributed to hydroxyls C–OH (287.5 \pm 0.1 eV) and carboxyls O=C–H (288.9 \pm 0.2 eV).^[9] The intensities of these peaks increased relative to the sp²-hybridized carbons due to the oxidation process. The XPS analysis of the C_{1s} spectrum of MWNT-NH₃⁺ indicated the presence of amide bonds N–C=O (287.9 eV) and amine C–N (286.2 eV),^[9,16] which suggested the successful formation of amide bonds and introduction of amine groups.

The colloidal stability of aqueous dispersions of MWNT-COO⁻ and MWNT-NH₃⁺ was determined using zeta potential analysis. Both functionalized MWNT suspensions are sufficiently stable across the studied pH range from 3 to 8, with zeta potential values of -43.3 mV (MWNT-COO⁻) at pH 4 and $+50.1$ mV (MWNT-NH₃⁺) at pH 4 (Figure S3, Supporting Information). With these stable MWNT suspensions, (MWNT-COO⁻/MWNT-NH₃⁺)_{*n*} films, where *n* denotes the number of film bilayers, were deposited on top of the (SPS/PDAC)₁₀ base layer by sequentially spraying MWNT-COO⁻ and MWNT-NH₃⁺ suspensions onto the ES fiber mat. Figure 1d shows top-down and cross-sectional SEM images of ES fiber mats coated with

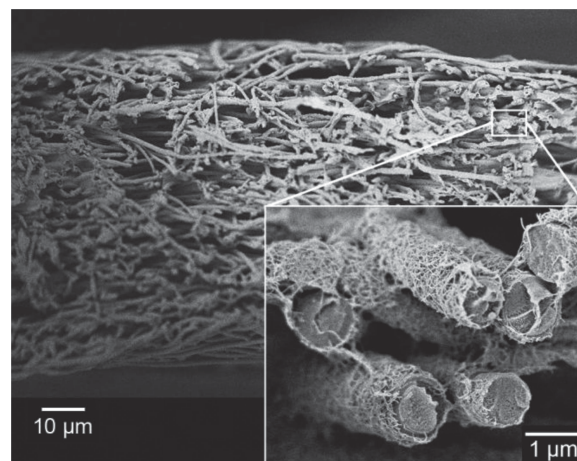


Figure 2. SEM images of entire cross-section of an electrospun fiber mat coated with 15 bilayers of (MWNT-COO⁻/MWNT-NH₃⁺) films (inset shows higher magnification view).

(MWNT-COO⁻/MWNT-NH₃⁺)₁₅. The SEM images show that the LbL-MWNT films were conformally coated on individual fibers with uniform cross-section, showing no preference toward the direction of fluid flow. Furthermore, SEM images of a cross-section of a coated ES fiber mat (Figure 2) demonstrate that the convective flow of MWNT suspension penetrated throughout the depth of the 103 ± 2 μm thick ES fiber mat, enabling uniform growth of MWNT films from the front to the back side of the substrate. The ES fiber mat also retained its flexibility after coating with the MWNT films (Figure S4, Supporting Information).

Figure 3a shows a series of SEM images consisting of an ES fiber coated with 2, 5, and 10 bilayers of (MWNT-COO⁻/MWNT-NH₃⁺), respectively. The SEM images clearly show that the MWNT loading increases with the number of deposited layers, gradually covering the ES fiber until the underlying fiber is not visible, as demonstrated for the films with 10 bilayers. The buildup of MWNT films on ES fibers was not observed when only a MWNT-COO⁻ suspension was used (Figure S5, Supporting Information), suggesting that an electrostatic cross-linking between positively and negatively charged MWNTs is the major driving force for the multilayer assembly process rather than simple film accumulation. The porous network structure of the MWNT films also shows that the electrostatic repulsion between well-dispersed nanotubes dominated the attractive Van der Waals forces, resulting in randomly oriented arrangements of unbundled MWNTs. Well-exposed tubes in the MWNT films increase the effective surface area available for interactions with surrounding molecules compared to more traditional methods of assembling nanotubes, making the MWNT coated ES fiber mat highly attractive as a CNT based electrode for sensor applications. Figure 3b displays the cumulative weight of (MWNT-COO⁻/MWNT-NH₃⁺) films on the ES fiber mat as a function of the number of bilayers. As expected for film thicknesses that are much less than the fiber diameter, a linear growth profile is observed, consistent with our previous observation for LbL-assembled films of MWNTs on a flat Si wafer.^[9] The sheet resistance of the MWNT/ES fiber electrodes

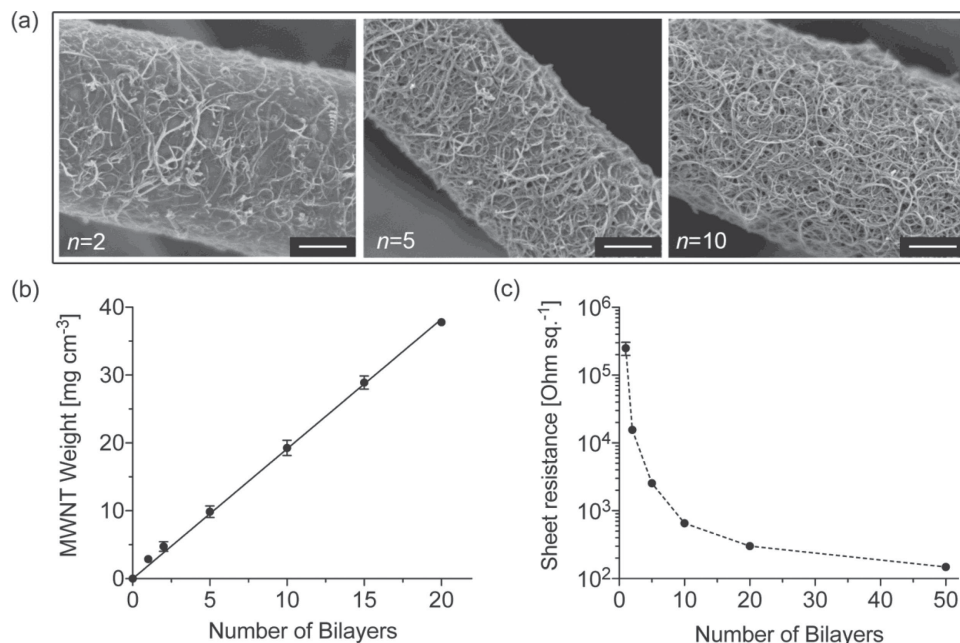


Figure 3. a) Scanning electron microscopy images of ES fibers coated with MWNT films, where n indicates the number of bilayers (2, 5, and 10, respectively) in $(\text{MWNT-COO}^-/\text{MWNT-NH}_3^+)_n$ films (scale bar, 400 nm). b) Correlation of cumulative weight [mg cm^{-3}] to layer pair number of MWNT films. The straight line is a linear fit. c) Sheet resistance [ohm square^{-1}] of the MWNT/ES fiber electrodes.

was measured by four-point probe and presented as a function of the number of bilayers (Figure 3c). The sheet resistance decreases with increasing number of bilayers, indicating that added layers of MWNT films enhance the conductivity of the composite material. The MWNT/ES fiber electrode underwent a transition from an electrically nonconductive to a conductive thin film after just one bilayer of $(\text{MWNT-COO}^-/\text{MWNT-NH}_3^+)$ film was deposited, suggesting that an interconnected network of MWNTs well above the percolation threshold was formed. The control over MWNT loading and conductivity of the MWNT/ES fiber electrodes demonstrate their potential use in energy and sensor devices.

The electrical conductivity (σ) of the MWNT/ES fiber electrodes was calculated from the sheet resistance according to Equation 2 and presented as a function of the volume fraction of MWNTs ($\Phi = V_{\text{MWNT}}/V_{\text{mat}}$) in the MWNT/ES fiber electrode (Figure 4). The volume of MWNTs (V_{MWNT}) was derived using the total weight of the composite electrode that is due to deposited MWNT films and the density of free-standing LbL-assembled MWNT films of 0.83 g cm^{-3} reported by Lee et al.^[9] The apparent volume of the polysulfone ES fiber mat (V_{mat}) was determined by measuring dimensions of the mat specimen.

$$\sigma = 1/(R_s T) \quad (2)$$

where R_s is sheet resistance, and T is thickness of MWNT/ES fiber electrode.

The conductivity value of $0.7 \pm 0.03 \text{ S cm}^{-1}$ for the MWNT/ES fiber electrode with 50 bilayers of LbL-MWNT films is of the same order of magnitude as the value of approximately 1 S cm^{-1} reported by Lee et al. for free-standing LbL-assembled MWNT films.^[9] The conductivity of the MWNT/ES fiber electrode increases dramatically after the percolation threshold

($\Phi_c = 0.0022$ at 1 bilayer) is reached and approaches a plateau with increasing MWNT loading. This behavior closely resembles the electrical conductivity of polymers reinforced with randomly distributed, electrically conductive particles. According to the percolation theory, a power law can describe the relationship between electrical conductivity of a composite material and conductive filler concentration

$$\sigma \propto (\Phi - \Phi_c)^\beta \quad (3)$$

where Φ is the volume fraction of conductive filler, Φ_c is the volume fraction at the percolation threshold, and β is the

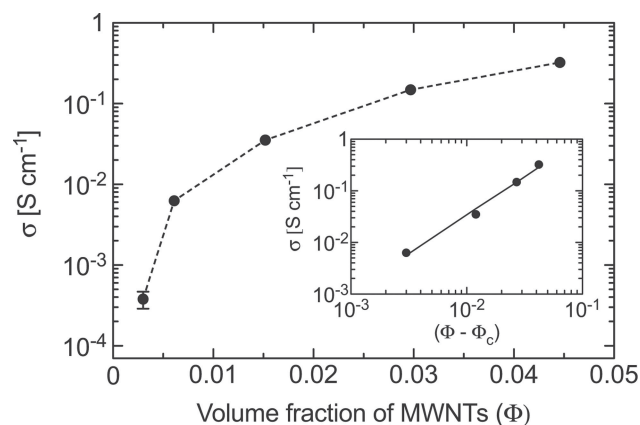


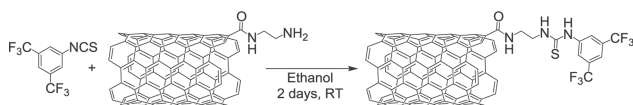
Figure 4. Electrical conductivity (σ) of MWNT/ES fiber electrode as a function of volume fraction of MWNTs (Φ). Insert: a log-log plot of σ versus reduced volume fraction of MWNTs, $(\Phi - \Phi_c)$. The solid line is a fit to a power law (Equation 3).

critical exponent, which reflects the dimensionality of the system. Theoretical values for β are around 1.33 and 2.0 for two and three-dimensional systems, respectively.^[17] The log-log plot (Figure 4 insert) of electrical conductivity versus reduced volume fraction of MWNTs, $(\Phi - \Phi_c)$, shows that the electrical conductivity of MWNT composite agrees well with the percolation behavior described by Equation 3. The best fit to experimental values resulted in $\beta = 1.5$. The low β suggests that the conductivity of the MWNT/ES fiber electrode behaves similarly to that of a two-dimensional lattice of a CNT film (network) on a flat substrate,^[18] consistent with the relatively thin nature of the films, ranging from approximately 15 to 100 nm in thickness. The percolation threshold (Φ_c) of approximately 0.22 vol% falls within the range of the values reported in literature for MWNT-epoxy composites (0.1 to 3.8 vol%).^[19] The aspect ratio and dispersion state of CNTs have a significant impact on the percolation threshold, resulting in the wide range of reported values.^[20] Balberg et al. used the excluded volume concept to describe a statistical distribution of conductive filler sticks shaped as capped cylinders and correlated the relationship between Φ_c and aspect ratio (η) as $\Phi_c \propto \eta^{-2}$ for $\eta > 15$.^[21] This dependence explains why the observed percolation threshold ($\Phi_c = 0.22$ vol%, $\eta \approx 60$ for MWNTs used in this work) is higher than that reported for other CNT-epoxy composites with higher aspect ratio CNTs (e.g., $\Phi_c = 0.0025$ wt% for $\eta \approx 340$).^[22a] but is still relatively low when compared to spherical particles ($\Phi_c = 16\%$).^[22b] such as carbon black, as anticipated.

2.2. Functionalization of Thiourea-Based Receptor to the MWNT/ES Fiber Electrode

The LbL-MWNT films deposited on the MWNT/ES fiber electrode are composed of carboxylic acid (MWNT-COO⁻) and amine (MWNT-NH₃⁺) functionalized MWNTs. These functional groups on the MWNT surfaces can be utilized for coupling other molecules directly to the surface of the MWNT/ES fiber electrode to tailor its functionality and properties. Here, the available -NH₂ functional groups on the surface of MWNT-NH₃⁺ were reacted with an electron poor isothiocyanate derivate to covalently attach a thiourea-based receptor on the MWNT/ES fiber electrode (Scheme 2).

The presence of the thiourea group is intended to promote strong interactions between the MWNT/ES fiber electrode and DMMP through the hydrogen-bonding affinity of thiourea ($pK_A = 21.1$ in DMSO)^[23] toward the phosphate ester in DMMP, which is common to G-type nerve agents. Specifically, the phosphate ester acts as a strong hydrogen-bond acceptor that binds to the acidic thiourea protons.^[24] The electron-withdrawing group (3, 5-bis(trifluoromethyl) phenyl) is expected



Scheme 2. Covalent attachment of thiourea group to the -NH₂ functional groups on the surface of MWNT-NH₃⁺ in the MWNT multilayer films. For clarity, a single-walled carbon nanotube segment is shown with only a single functional group at the end of the tube.

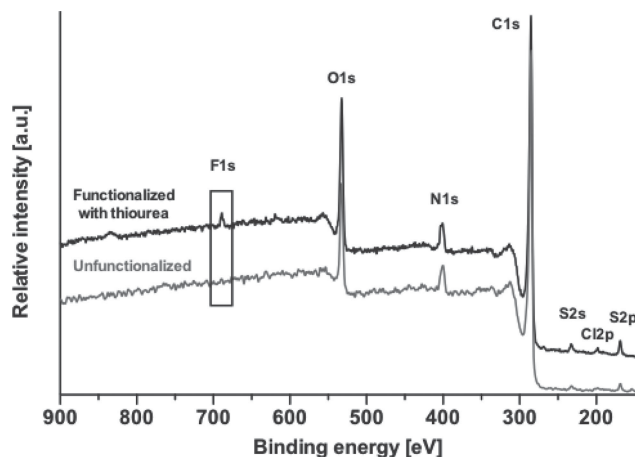


Figure 5. X-ray photoelectron survey spectra of ES fiber mats coated with (MWNT-COO⁻/MWNT-NH₃⁺)₂ films before and after functionalization with thiourea, showing the presence of O1s, N1s, C1s, S2s, S2p, and Cl2p. The appearance of fluorine (F1s) as highlighted in the box indicates the successful attachment of the thiourea functional group to the surface of MWNTs.

to increase the acidity of the thiourea protons and thus further strengthens the interactions of DMMP with the thiourea moiety. Figure 5 shows the X-ray photoelectron spectroscopy (XPS) survey spectra of an ES fiber mat coated with 2 bilayers of (MWNT-COO⁻/MWNT-NH₃⁺) films before and after functionalization with the thiourea unit. The XPS survey scans show the presence of C, O, and N, which are characteristic of the carboxyl and amine groups of MWNT-COO⁻ and MWNT-NH₃⁺, respectively. Sulfur peaks (S2s and S2p) can be assigned largely to the polysulfone electrospun fibers. Chlorine was present as expected from the chloride counterions in the LbL-MWNT films. Appearance of a F1s peak (atomic concentration $\approx 1\%$) after the functionalization suggests that the thiourea-based receptor, which contains a unique fluorine element, was successfully incorporated onto the MWNT/ES fiber electrode. Functional group density based on F1s and C1s signals by XPS was estimated to be 1 thiourea unit per 540 CNT carbons which approximately corresponded to 1 thiourea unit per 68 CNT carbons on the outer wall.

2.3. Response of Chemiresistive Sensor Based on MWNT/ES Fiber Electrode to DMMP

The MWNT/ES fiber electrodes (2 mm \times 10 mm) were integrated into a custom-made sensor enclosure (Figure 6a), for which the electrodes were electrically contacted with two platinum wires that were connected to a potentiostat. Figure 6b shows the current-voltage (I - V) curves of the MWNT/ES fiber electrodes that were coated with 2, 5, and 10 bilayers of (MWNT-COO⁻/MWNT-NH₃⁺) films. All MWNT/ES fiber electrodes exhibited ohmic behavior from their I - V characteristics. Although not measured, the contact resistance with the sensor enclosure was assumed to be small compared to the resistance of MWNT/ES fiber electrodes (0.2–0.5 M Ω). MWNT/ES fiber

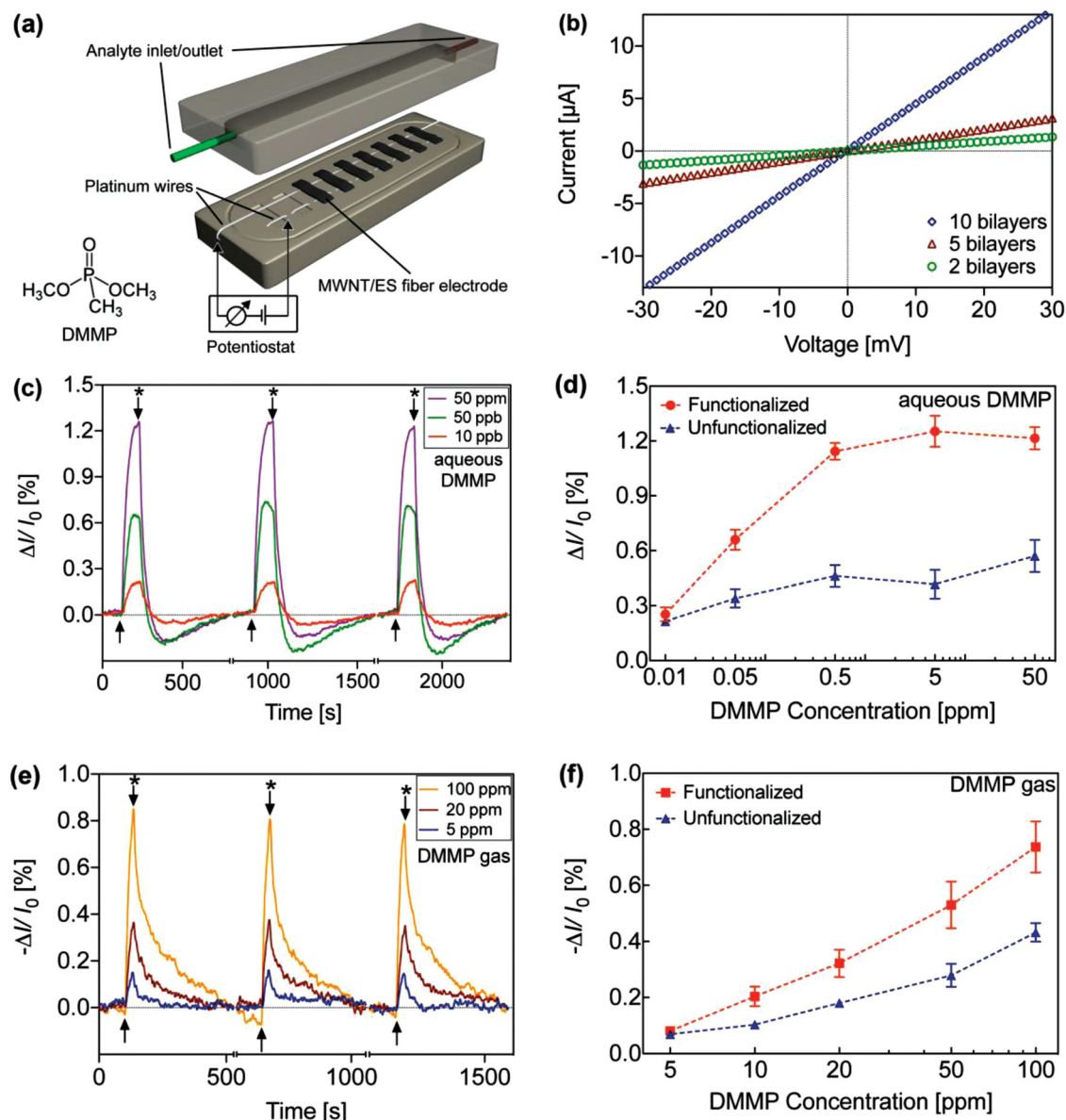


Figure 6. a) Schematic of the sensor device showing the MWNT/ES fiber electrodes enclosed in a custom-made flow chamber and electrical connectivity for current measurements. b) I - V characteristics of MWNT/ES fiber electrodes (scan rate, 1 mV s^{-1}). c) Variation of responses ($\Delta I/I_0$ [%]) of thiourea-functionalized MWNT/ES (TF-MWNT/ES) fiber electrode upon cyclic exposure to aqueous DMMP (10 ppb to 50 ppm) and water. DMMP is introduced at the arrow. The flow to the sensor is switched from DMMP to water at the arrow with the asterisk. d) Comparison of average responses of thiourea-functionalized and unfunctionalized MWNT/ES fiber electrodes as a function of aqueous DMMP concentration. e) Variation of responses of TF-MWNT/ES fiber electrodes upon cyclic exposure to diluted DMMP vapor (5, 20, 100 ppm) and nitrogen stream. DMMP is introduced at the arrow. The flow to the sensor is switched from DMMP to nitrogen at 'arrow with asterisk'. f) Comparison of average responses of thiourea-functionalized and unfunctionalized MWNT/ES fiber electrodes as a function of DMMP vapor concentration.

electrodes with more bilayers of the MWNT film also displayed higher electrical current because denser packing of MWNTs led to a lower resistance for electron transport across the conductive electrode. Using the sensor enclosure described above, the sensing capability of the thiourea-functionalized MWNT/ES (TF-MWNT/ES) fiber electrode (with two bilayers of (MWNT-COO⁻/MWNT-NH₃⁺) films) was investigated for detecting DMMP in both aqueous and vapor phases. The sensor signal ($S = (I - I_0)/I_0$ where I_0 is the initial current) is a normalized

change in electrical current monitored in real time between the two platinum wire electrodes at a constant voltage of 0.05 V. Figure 6c shows the sensor signal upon alternating exposure to aqueous DMMP solutions (100 s) and pure water (700 s) at varying concentrations (10 ppb to 5 ppm). Exposing aqueous DMMP to the TF-MWNT/ES fiber electrode caused the current to increase rapidly, then reach a plateau. The increase in electrical current of our MWNT sensor upon exposure to DMMP solution is consistent with observation by Roberts et al. for a

resistive sensor based on a single-walled carbon nanotube network.^[25] In an aqueous environment, a dipole interaction model is proposed as the mode of interaction between CNTs and DMMP because the polar DMMP has a strong dipole moment which can cause local induced-dipole electrostatic interactions between DMMP and carbon nanotubes.^[3c] After a pure water stream replaced DMMP, the current initially decreased below its original value and gradually recovered back to its initial level. We speculate this dip below the initial current can be attributed to swelling and/or relaxation of the polymer substrate when the flow was switched from DMMP to water. Exposing aqueous DMMP to a drop-cast film of thiourea-functionalized MWNTs that was deposited on a glass substrate did not elicit the drop in the current below the baseline value (Figure S6, Supporting Information). A normalized current change of 0.3% was observed in response to 10 ppb DMMP in water. This result is excellent sensitivity for MWNT based sensors operating in an aqueous environment. Our sensor was able to detect DMMP at concentration below the recommended maximum permissible concentration (MPC) for Sarin nerve agent in field drinking water of 14 ppb.^[26] The modulation in current was directly correlated to the concentration of DMMP, as shown Figure 6d. An approximately linear response was observed for the TF-MWNT/ES fiber electrodes to DMMP solution in the concentration range of 10 ppb to 0.5 ppm. A saturation of response was observed at concentrations above 0.5 ppm. The sensing response of the TF-MWNT/ES fiber electrodes to aqueous DMMP was compared to the unfunctionalized MWNT/ES fiber electrodes (Figure 6d). The TF-MWNT/ES fiber electrodes exhibited a 1.2–3.0-fold increase in the response when compared to the MWNT/ES fiber electrodes without the thiourea-based receptor. The improved response of the unfunctionalized MWNT/ES fiber electrodes to DMMP is expected, as a result of the hydrogen-bond interactions between DMMP molecules and the available carboxyl and amine groups on the unfunctionalized MWNT/ES fiber electrodes. DMMP, however, formed stronger hydrogen bonding with the acidic thiourea-NH protons on the TF-MWNT/ES fiber electrodes, resulting in a larger response. In addition, the observed response of the unfunctionalized MWNT/ES fiber electrodes showed little correlation with DMMP concentration. The enhancement in the sensory response through the functionalization of the thiourea-based receptor demonstrates the utility of the MWNT/ES fiber electrode as a platform for creating chemical/biological sensors.

The response of the TF-MWNT/ES fiber electrode was further examined upon cyclic exposures to different concentrations (5 to 100 ppm) of DMMP vapor (30 s) and N₂ stream (400 s). The sensing response (Figure 6e) gave a reduction in current (increase in resistance), which was reversible. The response was rapid with the introduction of DMMP vapor, and gradually recovered back to its original level when the flow was switched from DMMP to N₂. This decrease in conductance of the MWNT sensor upon exposure to DMMP vapor can be attributed to the adsorption of DMMP molecules onto the surface of MWNT network and the subsequent change of the inter-tube (junction) resistance.^[27] The sensor response to DMMP vapor was directly dependent on the concentration of DMMP, as shown in Figure 6f. The incorporation of the thiourea-based receptor on MWNT/ES fiber electrodes led to a 1.2–2.0-fold increase in

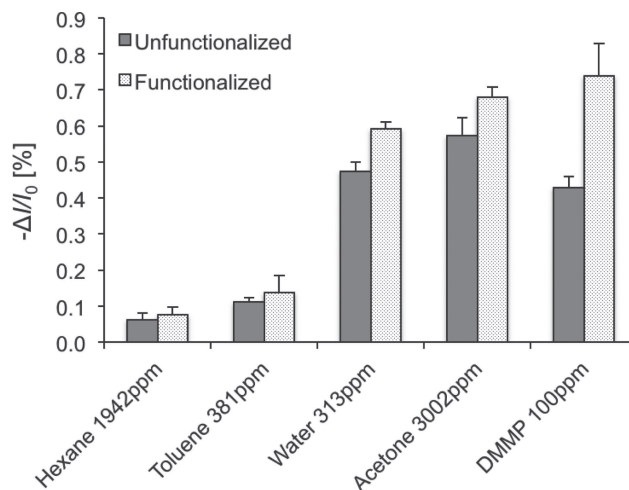


Figure 7. Average sensing response of unfunctionalized and thiourea-functionalized MWNT/ES fiber electrodes to different analytes. The concentration of each analyte represents 1% of its equilibrium vapor concentration at room temperature except DMMP, which was used at ≈6% of its equilibrium vapor concentration at room temperature.

response compared to the unfunctionalized MWNT/ES fiber electrodes.

The effect of the incorporation of the thiourea-based receptor was further evaluated by exposing the thiourea-functionalized and unfunctionalized MWNT/ES fiber electrodes to a variety of analytes (Figure 7). The thiourea-functionalized sensors showed a significant enhancement in sensing response to analytes that can form hydrogen-bonding interactions, for example, DMMP, acetone, and water. Non-polar analytes such as toluene and hexane induced a much lower response. These results are in line with the expected interaction of the tested analytes with the thiourea-functionalized and unfunctionalized MWNT/ES fiber electrodes. In this study, the thiourea-based moiety was the only receptor incorporated into the MWNT/ES fiber electrode; thus, the functionalized sensor was not designed for high selectivity. Adding different classes of receptors to the MWNT/ES fiber electrodes can improve sensor selectivity and will be investigated in the future.

The kinetics of adsorption and desorption of DMMP vapor on the sensors was modeled to extract kinetic parameters, such as the adsorption rate constant (k), desorption rate constant (k_{-1}), and equilibrium constant ($K = k/k_{-1}$). The desorption step was first fitted to a reversible binding model described elsewhere^[28a] using a first-order reaction rate to obtain k_{-1} , which is directly related to the DMMP desorption rate.^[28b] The desorption part of the sensor signal ($S = \Delta I/I_0$, where S_0 is the signal when the analyte is removed) was fitted to Equation 4 to obtain $k_{-1} = 1.7 \pm 0.2 \times 10^{-2} \text{ s}^{-1}$ for the thiourea-functionalized sensor and $2.6 \pm 0.4 \times 10^{-2} \text{ s}^{-1}$ for the unfunctionalized sensor (see Figure S7, Supporting Information, for curve-fitting). These values are within the range of previously reported values for DMMP desorption rate of $3.67 \times 10^{-4} \text{ s}^{-1}$ and 0.525 s^{-1} for resistive sensors based on single-walled carbon nanotubes.^[7,28a] The desorption rate of the unfunctionalized sensor is 55% higher than the value obtained for the thiourea-functionalized sensor. This result

suggests that the presence of the thiourea-based receptor slowed down the desorption process of DMMP molecules because DMMP interacted more strongly with the sensor with the thiourea-based receptor. Fitting the adsorption portion of the data to a reversible binding kinetic model, as described elsewhere,^[28a] Equation 5, at an analyte concentration C_A , gives $k = 9.7 \pm 0.5 \times 10^{-7} \text{ ppb}^{-1} \text{ s}^{-1}$ and $K = 7.3 \pm 0.7 \times 10^{-5} \text{ ppb}^{-1}$ for the thiourea-functionalized sensor, and $k = 4.9 \pm 0.4 \times 10^{-7} \text{ ppb}^{-1} \text{ s}^{-1}$ and $K = 3.2 \pm 0.5 \times 10^{-5} \text{ ppb}^{-1}$ for the unfunctionalized sensor. The K value of the thiourea-functionalized sensor is very close to the previously reported equilibrium constant of $6.98 \times 10^{-5} \text{ ppb}^{-1}$ as reported by Lee et al.^[28b] for a DMMP gas sensor based on functionalized single-walled carbon nanotubes.

$$S(t) = S_0 \exp(-k_{-1}t) \quad (4)$$

$$S(t) = \left(\frac{kC_A}{(kC_A + k_{-1})} \right) (1 - \exp(-(kC_A + k_{-1})t)) \quad (5)$$

3. Conclusions

We have presented a versatile, scalable method for depositing conformal, binder-free MWNT multilayer films on flexible, porous electrospun (ES) fiber substrates. The vacuum-assisted spray-LbL assembly technique enables rapid, uniform electrostatic assembly of positively and negatively charged MWNTs on individual ES fibers, creating highly porous networks of conformal MWNT multilayers with controlled loading and electrical conductivity. The available $-\text{NH}_2$ and $-\text{COOH}$ functional groups on the MWNT films offer a direct route for covalently attaching a receptor of interest to the MWNTs, in order to tailor the chemical specificity of the MWNT/ES fiber electrode for sensing applications and a means of greatly increasing properties such as selectivity and sensitivity in a modular fashion. Here, a thiourea-based receptor was covalently attached to the $-\text{NH}_2$ functional groups on the MWNT/ES fiber electrodes to enhance sensitivity toward DMMP, resulting in an up to 3-fold increase in sensing response when compared to unfunctionalized MWNT/ES fiber electrodes and very high levels of sensitivity for aqueous multi-walled carbon nanotube sensors. This work shows that the engineered textile can function as an ultra-sensitive sensing platform for real-time detection of an analyte of interest in an aqueous or gas phase. More importantly, this work demonstrates another example of the simple, versatile, water-based method of spray-LbL coating for introducing new functionalities to complex three-dimensional structures. We believe this method will provide an economical, yet powerful tool for developing lightweight, flexible carbon-nanotube-based sensors, intelligent textiles and wearable electronics.

4. Experimental Section

Materials: All chemicals, unless stated otherwise, were purchased from Sigma Aldrich (St. Louis, MO) and used without further purification. pH adjustment of all solutions was done by addition of dilute hydrochloric acid or sodium hydroxide. Poly(sodium 4-styrenesulfonate) (SPS, $M_w = 70\,000$) and poly(diallyldimethylammonium chloride) (PDAC,

$M_w = 150\,000$, 20% aqueous solution) were prepared as 0.01 M solutions, on the basis of the repeat-unit molecular weight, in deionized water (Milli-Q, 18.2 M Ω cm) and titrated to pH 4. Branched polyethylenimine (BPEI, $M_w = 75\,000$) was purchased from PolySciences (Warrington, PA). Pristine MWNTs (95% purity, length 1–5 μm , outer diameter $15 \pm 5 \text{ nm}$) synthesized by chemical vapor deposition were purchased from NanoLab (Newton, MA).

Preparation of Electrospun Fiber Materials: The electrospinning apparatus used is similar to a previous report;^[12] briefly, it consists of two aluminum disks 10 cm in diameter oriented parallel to each other and separated by a distance of 30 cm. A 25 wt% solution of bisphenol A polysulfone (UDEL P3500, Solvay Advanced Polymers) in 1:1 N,N-dimethyl formamide (DMF):N-methylpyrrolidone (NMP) is pumped through a Teflon tube with a syringe pump (Harvard Apparatus PHD 2000) at a rate of 0.010 mL min⁻¹ through a 0.040" ID needle in the top aluminum disk. A power supply provides 18.0 kV potential to the upper aluminum disk and the polymer solution is drawn to the bottom grounded disk where fibers of $1.69 \pm 0.17 \mu\text{m}$ in diameter are collected. The thickness of the mat can be controlled by the time allowed deposition (2 h for ca. 100 μm thick mat), after which the sample is annealed in an oven at 150 °C for 2 h in order to remove any residual solvent as well as to improve the strength of the electrospun (ES) fiber mat. Mean and standard deviation of fiber diameter were determined from measurements, using ImageJ,^[12] of 100 fibers selected manually and at random from an SEM image with a magnification of 5000 \times . The thickness of the ES mat was measured by a digital micrometer (Mitutoyo CLM1) with a constant measuring force of 0.5 N. Prior to LbL deposition, 2.5-inch diameter disk of polysulfone ES mat was cut and treated with one minute of air plasma (Harrick PDC-32 G plasma cleaner) to improve the wettability by introducing charged carboxylated groups on the surface. The mat was then immediately immersed into a 0.2 wt% aqueous solution of BPEI for 10 min to impart positive charge on the surface of ES fibers.

Functionalization of MWNTs: MWNTs modified with negatively charged carboxylate ions (MWNT-COO⁻) were prepared by an oxidation treatment according to a published protocol.^[9] MWNTs were refluxed in strong acids (3/1 v/v, 95% H₂SO₄, 70% HNO₃) at 70 °C for 2 h, and then washed several times with deionized water by filtration using a polypropylene carbonate membrane (Whatman, pore size = 50 nm). The MWNT-COO⁻ powder was dispersed in deionized water to attain 0.5 mg mL⁻¹ suspension. The resulting suspension was dialyzed (MWCO 6000–8000) for a few days to remove any residuals and byproducts from functionalization. MWNTs modified with positively charged ammonium ions (MWNT-NH₃⁺) were prepared as previously reported by reacting MWNT-COO⁻ suspension (400 mL, 0.5 mg mL⁻¹) with excess ethylenediamine (40 mL) in the presence of 4 g of 1-[3-(Dimethylamino)propyl]-3-ethylcarbodiimide methiodide.^[10] The resulting suspension was also dialyzed for a few days to remove any residuals and byproducts. The pHs of MWNT suspensions were adjusted after synthesis and sonicated (Branson Bransonic 2510 ultrasonic cleaner) briefly prior to LbL assembly.

LbL Film Assembly: Conformal (MWNT-COO⁻/MWNT-NH₃⁺)_n films were coated on ES fibers using a vacuum-assisted spray-LbL technique with a modification of the reported protocol.^[8a] Typically, a 2.5-inch diameter disk of polysulfone ES mat was placed on a stainless steel mesh (56 mesh, 0.004", TWP Inc.) and fixed inside a modified filter holder (Pall Life Science) by a cap. The back of the filter holder was connected via rubber tubing to a vacuum source to create airflow through the ES mat during spray deposition. All solutions were atomized into spray and delivered by a home-built automated spray system using high purity N₂ (20 psi). A base film of (SPS/PDAC)₁₀ was deposited on the ES mat with the following steps. SPS solution (0.01 M, pH 4) was sprayed for 4 s at a rate of 0.3 mL s⁻¹ and drained for 10 s under vacuum. Subsequently, pH 4 rinse water was sprayed for 4 s and drained for 10 s under vacuum. This half cycle was repeated for PDAC solution (0.01 M, pH 4) to complete one bilayer of (SPS/PDAC) film. The total cycle (56 s) was repeated 10 times to complete the base layers. (MWNT-COO⁻/MWNT-NH₃⁺)_n films were deposited on top of

the (SPS/PDAC)₁₀ base layers by repeating the above procedure with an increased drain time of 90 s, resulting in about a 4 min process cycle to complete one layer of (MWNT-COO⁻/MWNT-NH₃⁺) film. The total number of cycles, *n*, was adjusted to achieve a target number of film layers.

Characterization: The surface chemistry of functionalized MWNTs and MWNT film-coated ES fibers was analyzed using a Kratos AXIS Ultra Imaging X-ray photoelectron spectrometer (XPS). Zeta potential of MWNT aqueous suspension was measured using a Zeta PALS instrument (Brookhaven Instrument Corp.). MWNT mass loading was measured by weighing the ES mat before and after coating with MWNT films using a micro-balance (Sartorius M2P). Sheet resistance of MWNT coated ES mats was measured using a four-point probe method (Keithley SCS-4200). Four measurements were taken on each film, and the measurements were averaged to give the final reported value with the standard deviation. Morphologies of the surfaces and the cryo-fractured cross-sections of LBL films were examined using a scanning electron microscope (JEOL 6320FV Field-Emission High-Resolution SEM) operating at 2 and 5 kV.

Functionalization of MWNT/ES Fiber Electrode with Thiourea-Based Receptor: The MWNT-film coated ES mat was cut into rectangles (2 mm × 10 mm). Subsequently, the rectangles were immersed separately in 1-isothiocyanato-3,5-bis(trifluoromethyl)benzene solution (1 mL of 0.09 M isothiocyanate solution in ethanol). After 4 d, 1 mL of isocyanate solution was added (0.09 M in ethanol). After 6 additional hours, the liquid was removed and the film was washed six times by immersion in ethanol (2.5 mL each), followed by immersion in ethanol (three times, 15 mL ethanol each) and sonication for 3 times 5 s in 1.5 mL ethanol. The last washing solution was tested for isocyanate via thin layer chromatography (TLC), showing no residual reagent or other UV-active impurities. The functionalized mats were air dried overnight and then heat-treated at 150 °C for 12 h in vacuum to improve film stability.

Procedure for Sensing Measurements: The MWNT/ES fiber electrodes (2 mm × 10 mm) were placed inside a homemade flow chamber. The electrodes made electrical contacts with platinum wires (5 mm apart) to connections on the outside of the chamber. Two ports on opposite ends of the chamber allowed continuous flow of liquid or gas through the chamber. Up to 9 samples could be tested simultaneously. Two samples were used for each measurement. For aqueous sensing measurements, the inlet was attached to a tubing system with a Y connector attached to two syringes (Figure S8, Supporting Information). The two syringes were controlled using two separate syringe pumps (Harvard Apparatus, Holliston, MA) with a constant flow rate of 0.5 mL min⁻¹. In a typical aqueous sensing measurement, the MWNT/ES fiber electrodes were first exposed to MilliQ water. The flow was then switched from water to diluted DMMP solution for 100 s and changed back to MilliQ water for 700 s. In each test, the MWNT/ES fiber electrodes were exposed to at least three pulses of DMMP solution. For gas sensing measurements, the chamber inlet was connected a KIN-TEK gas generator system where a DMMP/nitrogen gas mixture was generated. A trace amount of DMMP vapor produced in a heated chamber at 70 °C was mixed with a nitrogen stream to create an oven flow, which was further diluted with another nitrogen stream (dilution flow) to achieve a target concentration. In a typical gas sensing measurement, the MWNT/ES fiber electrodes were first exposed to dilution flow. Subsequently, a mixture of oven and dilution flows was run through the device for 30 s, followed by dilution flow for 400 s. Electrochemical measurements were conducted using a PalmSens potentiostat connected to a laptop computer and controlled through PSTrace software. Electrical current was monitored in real time at an applied voltage of 0.05 V.

Supporting Information

Supporting Information is available from the Wiley Online Library or from the author.

Acknowledgements

This research was supported by the US Army through the Institute for Soldier Nanotechnologies under contract DAAD-19-02-0002 with the US Army Research Office. The content does not necessarily reflect the position of the government, and no official endorsement should be inferred. The authors also thank the Institute for Soldier Nanotechnologies and Center for Materials Science and Engineering (CMSE) at MIT for the use of facilities for electron microscopy and XPS work.

Received: July 12, 2013

Published online: September 20, 2013

- [1] P. Lukowicz, T. Kirstein, G. Troster, *Method Inform. Med.* **2004**, *43*, 232.
- [2] a) K. Nomura, H. Ohta, A. Takagi, T. Kamiya, M. Hirano, H. Hosono, *Nature* **2004**, *432*, 488; b) J. R. Windmiller, J. Wang, *Electroanalysis* **2013**, *25*, 29; c) L. B. Hu, M. Pasta, F. La Mantia, L. F. Cui, S. Jeong, H. D. Deshazer, J. W. Choi, S. M. Han, Y. Cui, *Nano Lett.* **2010**, *10*, 708; d) M. C. McAlpine, H. Ahmad, D. W. Wang, J. R. Heath, *Nat. Mater.* **2007**, *6*, 379.
- [3] a) J. Kong, N. R. Franklin, C. W. Zhou, M. G. Chapline, S. Peng, K. J. Cho, H. J. Dai, *Science* **2000**, *287*, 622; b) J. P. Novak, E. S. Snow, E. J. Houser, D. Park, J. L. Stepnowski, R. A. McGill, *Appl. Phys. Lett.* **2003**, *83*, 4026; c) E. S. Snow, F. K. Perkins, E. J. Houser, S. C. Badescu, T. L. Reinecke, *Science* **2005**, *307*, 1942; d) F. Wang, H. W. Gu, T. M. Swager, *J. Am. Chem. Soc.* **2008**, *130*, 5392; e) E. S. Snow, F. K. Perkins, J. A. Robinson, *Chem. Soc. Rev.* **2006**, *35*, 790.
- [4] S. Park, M. Vosguerichian, Z. A. Bao, *Nanoscale* **2013**, *5*, 1727.
- [5] a) X. Y. Wang, Y. G. Kim, C. Drew, B. C. Ku, J. Kumar, L. A. Samuelson, *Nano Lett.* **2004**, *4*, 331; b) D. Bhattacharyya, K. Senecal, P. Marek, A. Senecal, K. K. Gleason, *Adv. Funct. Mater.* **2011**, *21*, 4328.
- [6] a) G. Decher, *Science* **1997**, *277*, 1232; b) P. T. Hammond, *Mater. Today* **2012**, *15*, 196.
- [7] a) P. T. Hammond, *Aiche J.* **2011**, *57*, 2928; b) S. S. Shiratori, M. F. Rubner, *Macromolecules* **2000**, *33*, 4213; c) J. Choi, M. F. Rubner, *Macromolecules* **2005**, *38*, 116.
- [8] a) K. C. Krogman, J. L. Lowery, N. S. Zacharia, G. C. Rutledge, P. T. Hammond, *Nat. Mater.* **2009**, *8*, 512; b) D. S. Liu, J. N. Ashcraft, M. M. Mannarino, M. N. Silberstein, A. A. Argun, G. C. Rutledge, M. C. Boyce, P. T. Hammond, *Adv. Funct. Mater.* **2013**, *23*, 3087.
- [9] S. W. Lee, B. S. Kim, S. Chen, Y. Shao-Horn, P. T. Hammond, *J. Am. Chem. Soc.* **2009**, *131*, 671.
- [10] S. Y. Kim, J. Hong, R. Kaviani, S. W. Lee, M. N. Hyder, Y. Shao-Horn, P. T. Hammond, *Energy Environ. Sci.* **2013**, *6*, 888.
- [11] a) K. Zhou, G. A. Thouas, C. C. Bernard, D. R. Nisbet, D. I. Finkelstein, D. Li, J. S. Forsythe, *ACS Appl. Mater. Interfaces* **2012**, *4*, 4524; b) L. M. He, P. P. Zhao, Q. Han, X. Y. Wang, X. Cai, Y. F. Shi, L. B. Zhou, Y. M. Zhang, W. Xue, *Carbon* **2013**, *56*, 224; c) Y. Luo, S. G. Wang, M. W. Shen, R. L. Qi, Y. Fang, R. Guo, H. D. Cai, X. Y. Cao, H. Tomas, M. F. Zhu, X. Y. Shi, *Carbohydr. Polym.* **2013**, *91*, 419.
- [12] M. M. Mannarino, G. C. Rutledge, *Polymer* **2012**, *53*, 3017.
- [13] a) G. C. Kapantaidakis, G. H. Koops, *J. Membr. Sci.* **2002**, *204*, 153; b) V. Deimede, G. A. Voyiatzis, J. K. Kallitsis, L. Qingfeng, N. J. Bjerrum, *Macromolecules* **2000**, *33*, 7609.
- [14] K. Asfardjani, Y. Segui, Y. Aurelle, N. Abidine, *J. Appl. Polym. Sci.* **1991**, *43*, 271.
- [15] W. M. Deen, *Analysis of Transport Phenomena*; 6th ed., Oxford University Press, New York **1998**.

- [16] T. Ramanathan, F. T. Fisher, R. S. Ruoff, L. C. Brinson, *Chem. Mater.* **2005**, *17*, 1290.
- [17] a) M. Weber, M. R. Kamal, *Polym. Compos.* **1997**, *18*, 711; b) D. Stauffer, A. Aharony, *Introduction to Percolation Theory*, Taylor & Francis, London **1992**.
- [18] L. B. Hu, D. S. Hecht, G. Gruner, *Chem. Rev.* **2010**, *110*, 5790.
- [19] a) J. H. Du, L. Zhao, Y. Zeng, L. L. Zhang, F. Li, P. F. Liu, C. Liu, *Carbon* **2011**, *49*, 1094; b) Q. Li, Q. Z. Xue, L. Z. Hao, X. L. Gao, Q. B. Zheng, *Compos. Sci. Technol.* **2008**, *68*, 2290; c) B. Lin, U. Sundararaj, P. Potschke, *Macromol. Mater. Eng.* **2006**, *291*, 227; d) X. W. Jiang, Y. Z. Bin, M. Matsuo, *Polymer* **2005**, *46*, 7418; e) E. Logakis, C. Pandis, V. Peoglos, P. Pissis, J. Pionteck, P. Potschke, M. Micusik, M. Omastova, *Polymer* **2009**, *50*, 5103.
- [20] J. Li, P. C. Ma, W. S. Chow, C. K. To, B. Z. Tang, J. K. Kim, *Adv. Funct. Mater.* **2007**, *17*, 3207.
- [21] I. Balberg, C. H. Anderson, S. Alexander, N. Wagner, *Phys. Rev. B* **1984**, *30*, 3933.
- [22] a) J. K. W. Sandler, J. E. Kirk, I. A. Kinloch, M. S. P. Shaffer, A. H. Windle, *Polymer* **2003**, *44*, 5893; b) I. Balberg, N. Binenbaum, *Phys. Rev. B* **1987**, *35*, 8749.
- [23] F. G. Bordwell, *Acc. Chem. Res.* **1988**, *21*, 456.
- [24] Y. B. Jiang, A. F. Li, J. H. Wang, F. Wang, *Chem. Soc. Rev.* **2010**, *39*, 3729.
- [25] M. E. Roberts, M. C. LeMieux, Z. N. Bao, *ACS Nano* **2009**, *3*, 3287.
- [26] *Guidelines for Chemical Warfare Agents in Military Field Drinking Water*, National Academies Press, Washington, D.C. **1995**.
- [27] F. Wang, T. M. Swager, *J. Am. Chem. Soc.* **2011**, *133*, 11181.
- [28] a) C. Y. Lee, M. S. Strano, *Langmuir* **2005**, *21*, 5192; b) C. Y. Lee, R. Sharma, A. D. Radadia, R. I. Masel, M. S. Strano, *Angew. Chem. Int. Ed.* **2008**, *47*, 5018.